Quantum dynamics of an atom orbiting around an optical nanofiber

Fam Le Kien,[1,2,*] K. Hakuta,[1] D. Reitz,[2] P. Schneeweiss,[2] and A. Rauschenbeutel[2]

[1]*Center for Photonic Innovations, University of Electro-Communications, Chofu, Tokyo 182-8585, Japan*

[2]*Vienna Center for Quantum Science and Technology, TU Wien – Atominstitut, Stadionallee 2, 1020 Vienna, Austria*

(Received 12 September 2012; revised manuscript received 10 May 2013; published 7 June 2013)

We propose a platform for the investigation of quantum wave-packet dynamics, offering a complementary approach to existing theoretical models and experimental systems. It relies on laser-cooled neutral atoms which orbit around an optical nanofiber in an optical potential produced by a red-detuned guided light field. We show that the atomic center-of-mass motion exhibits genuine quantum effects like collapse and revival of the atomic wave packet. As distinctive advantages, our approach features a tunable dispersion relation as well as straightforward readout for the wave-packet dynamics and can be implemented using existing quantum optics techniques.

DOI: 10.1103/PhysRevA.87.063607 PACS number(s): 03.75.−b, 03.65.Ge, 37.10.Gh, 37.10.Vz

I. INTRODUCTION

Since the earliest days of quantum mechanics, the study of localized, time-dependent solutions to bound-state problems has attracted considerable attention [1]. Quantum mechanical objects show both particlelike and wavelike behavior and this duality can be readily explored by analyzing the dynamics of wave packets. Such localized states behave like classical objects and follow classical trajectories as long as they do not disperse. However, for nonlinear dispersion relations, the wave packet will spread out and the dynamics cannot be described anymore using classical physics. One of the most prominent witnesses of genuine quantum mechanical dynamics is when the collapse of the wave packet is followed by a revival, i.e., a relocalization of the wave function [2,3]. This intriguing quantum effect has been experimentally observed in a number of systems (see [3] and references therein), and dispersion engineering of wave packets as well as their collapse and revival dynamics constitute an active field of current research [4–6].

Here, we propose an experimental platform for the investigation of quantum wave-packet dynamics, offering a complementary approach to existing theoretical models and experimental systems. Our approach features a tunable dispersion relation as well as straightforward readout for the wave-packet dynamics and can be implemented using existing quantum optics techniques. It relies on laser-cooled neutral atoms which are interfaced with an optical nanofiber as initially proposed in Ref. [7] and thoroughly analyzed in Ref. [8]. In this scenario, an atom orbiting around the nanofiber can show quantum mechanical dynamics including an initially classical orbiting motion of the atomic wave packet around the nanofiber, a spread of the atomic wave function (collapse), a partial relocalization of the atom (fractional revival) [9], and, finally, a full quantum revival of the original wave packet. In the following, we study this dynamics quantitatively, give analytical expressions for relevant time scales, and derive the functional dependence of the expected signals when absorptively probing the dynamics using a nanofiber-guided, resonant light field.

*kien.pham@ati.ac.at; also at Institute of Physics, Vietnamese Academy of Science and Technology, Hanoi, Vietnam.

II. MODEL AND ANALYSIS

Consider an atom moving in vacuum around a silica nanofiber in a cylindrically symmetric potential $U(r)$; see Fig. 1. We use cylindrical coordinates $\{r,\varphi,z\}$, with z being the axis of the nanofiber. Due to the cylindrical symmetry of the system, the angular momentum $L_z = -i\hbar\partial/\partial\varphi$ of the atom with respect to the fiber axis z is conserved. In the eigenstate problem, we have $L_z = \hbar m$, where $\hbar$ is the reduced Planck constant and m is an integer, called the azimuthal quantum number. Hence, the atom's center-of-mass (COM) motional eigenstates can be written as $\Psi_{\nu mK} = (2\pi)^{-1} R_{\nu m}(r) e^{im\varphi} e^{iKz}$. Here, ν is the radial vibrational quantum number, K is the wave number of the matter wave along the z direction, and $R_{\nu m}(r)$ is the radial part of the wave function. We perform the transformation $R_{\nu m}(r) = u_{\nu m}(r)/\sqrt{r}$. The function $u_{\nu m}(r)$ is determined by the equation,

$$\left[-\frac{\hbar^2}{2M}\frac{\partial^2}{\partial r^2} + U_{\rm eff}^{(m)}(r)\right] u_{\nu m}(r) = \mathcal{E}_{\nu m} u_{\nu m}(r), \qquad (1)$$

where M is the atomic mass, $U_{\rm eff}^{(m)}(r) = U_{\rm cf}^{(m)}(r) + U(r)$ is the effective potential, with the centrifugal potential $U_{\rm cf}^{(m)}(r) = \hbar^2(m^2 - 1/4)/(2Mr^2)$, while $\mathcal{E}_{\nu m}$ is the energy eigenvalue for the COM motion of the atom transverse to the fiber. Thus, the radial motion of the atom orbiting around the nanofiber can be reduced to the motion of a particle in the one-dimensional effective potential $U_{\rm eff}^{(m)}(r)$.

There exist stable bound states for the atom if the effective potential $U_{\rm eff}^{(m)}$ has a local minimum outside of the fiber [8]. This may happen if U is attractive, opposite to the centrifugal potential $U_{\rm cf}^{(m)}$. In order to produce a cylindrically symmetric attractive potential, we send a circularly polarized red-detuned optical field of frequency ω through the nanofiber. When the nanofiber radius a is small enough, the fiber can support only the fundamental mode $\rm HE_{11}$ [10], which generates an evanescent-wave guided light field around the nanofiber.

The optical potential for the atom is given by $U_{\rm opt} = -\alpha(\omega)|\mathbf{E}|^2/4$, where $\alpha(\omega)$ is the real part of the atomic polarizability at the optical frequency ω and $\mathbf{E}$ is the positive-frequency component of the electric part of the guided light field. The details of the calculations of the optical potential $U_{\rm opt}$ for a cesium atom in the vicinity of a nanofiber can be found in Refs. [8,11]. We also take into account the attractive

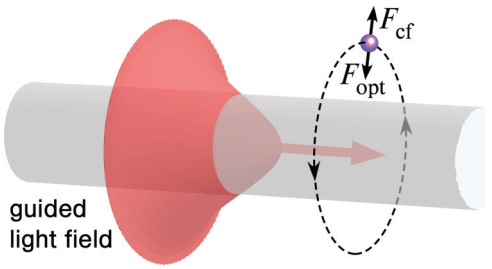

FIG. 1. (Color online) Schematic of trapping an atom in an orbit around an optical nanofiber by the evanescent wave of a quasicircularly polarized red-detuned guided light field.

fiber-induced van der Waals potential U_{vdW} of the atom [8,11]. The combination of the optical potential and the van der Waals potential yields the potential $U = U_{opt} + U_{vdW}$.

We plot in Figs. 2(a)–2(c) the effective potential $U_{eff}^{(m)}$ and the ground-vibrational-state eigenfunction $u_m \equiv u_{v=1,m}$ for a cesium atom in its electronic ground state orbiting around the nanofiber with the azimuthal quantum number m. In the following, the fiber radius is 200 nm and the wavelength and power of the trapping light are 1064 nm and 20 mW, respectively. We note that these parameters are well accessible experimentally [12,13]. Our calculations show that a trapping potential with a minimum outside the fiber can be formed when the azimuthal quantum number m is in the range from 430 to 530. We find that, in this region, the ground-vibrational-state energy $\mathcal{E}_m \equiv \mathcal{E}_{v=1,m}$ increases with increasing m and exhibits a small negative curvature; see Fig. 2(d). We note that we can tune the dispersion relation by varying the power of the guided light field, its wavelength, and/or the fiber radius.

In the following, the motion of the atom along the fiber axis is disregarded because it is independent of the motion in the fiber transverse plane and, consequently, independent of the azimuthal quantum number m. Let $|\psi_m\rangle$ be the ground state of

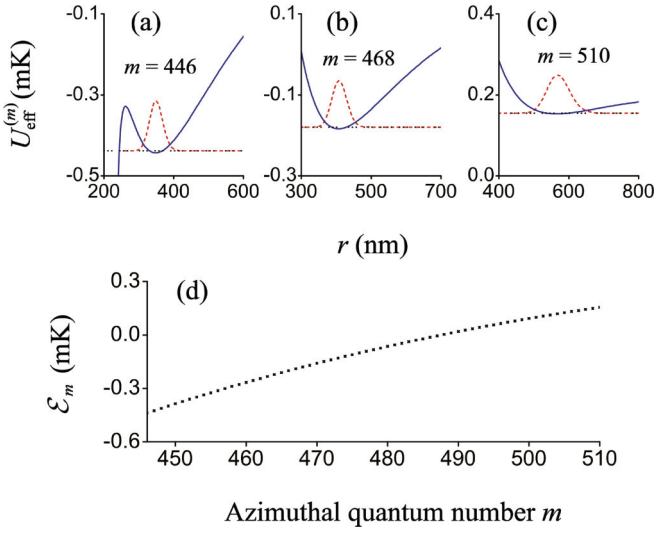

FIG. 2. (Color online) Effective potential $U_{eff}^{(m)}$ (solid blue lines) and ground-vibrational-state eigenfunction u_m (dashed red lines) for a ground-state cesium atom orbiting with the azimuthal quantum number $m = 446$ (a), 468 (b), and 510 (c) around the nanofiber. (d) Dispersion relation of the ground-vibrational-state energy $\mathcal{E}_m$.

the atomic COM motion transverse to the fiber with the angular momentum $\hbar m$. The wave function of this angular momentum state is $\psi_m(\mathbf{r}) = (2\pi r)^{-1/2} u_m(r) e^{im\varphi}$ and the corresponding energy is $\mathcal{E}_m$. Here, we have introduced the notation $\mathbf{r} = \{r,\varphi\}$. Consider a wave packet $|\psi\rangle = \sum_m c_m |\psi_m\rangle$, which is a linear superposition of the angular momentum states $|\psi_m\rangle$ with the corresponding probability amplitudes c_m. The temporal evolution of this superposition state is given by the wave function,

$$\psi(\mathbf{r},t) = \sum_m c_m e^{-i\mathcal{E}_m t/\hbar} \psi_m(\mathbf{r}). \tag{2}$$

We assume that the amplitudes of the individual angular momentum states are of the standard Gaussian distribution form, $c_m = (2\pi\Delta m^2)^{-1/4} \exp[-(m-m_0)^2/4\Delta m^2]$, with a peak at m_0 and a standard deviation Δm, and are truncated at $m_{min} < m_0$ and $m_{max} > m_0$. In our numerical calculations, we use $m_0 = 468$, $\Delta m = 6$, $m_{min} = 446$, and $m_{max} = 510$.

Since we have $m_0 \gg \Delta m \gg 1$, we can expand $\mathcal{E}_m$ in a Taylor series around m_0 according to

$$\mathcal{E}_m \cong \mathcal{E}_{m_0} + \mathcal{E}'_{m_0}(m-m_0) + \mathcal{E}''_{m_0}(m-m_0)^2/2, \tag{3}$$

where $\mathcal{E}'_m = d\mathcal{E}_m/dm$ and $\mathcal{E}''_m = d^2\mathcal{E}_m/dm^2$. In our case, we have $|\mathcal{E}''_{m_0}| \ll \mathcal{E}'_{m_0}$ which leads to the existence of two different time scales. Inserting Eq. (3) into Eq. (2) then allows one to identify these relevant time scales of the evolution of the wave packet [3]. The classical period of the rotation of the wave packet in the fiber transverse plane is given by $T_{rot} = 2\pi\hbar/\mathcal{E}'_{m_0}$. The characteristic collapse time is defined as the time at which the spread of phase differences between the various oscillatory terms in Eq. (2) is about π, that is, when the interference is most destructive. This characteristic time is given by $T_{coll} = 2\sqrt{\pi}\hbar/(|\mathcal{E}''_{m_0}|\Delta m)$. The revival time for the atomic wave packet is defined as the time at which the phase difference between two neighboring terms in Eq. (2) is 2π, that is, when the interference is most constructive. It is given by $T_{rev} = 4\pi\hbar/|\mathcal{E}''_{m_0}|$. For the parameters used in our numerical calculations, we have $\mathcal{E}'_{m_0}/2\pi\hbar \cong 214$ kHz and $|\mathcal{E}''_{m_0}|/2\pi\hbar \cong 2.52$ kHz, which lead to $T_{rot} \cong 4.67$ μs, $T_{coll} \cong 37.3$ μs, and $T_{rev} \cong 794$ μs.

We plot in Fig. 3 the spatial profiles of the atomic probability density $|\psi(\mathbf{r},t)|^2$ in the fiber transverse plane for different evolution times. Initially, at $t = 0$, the wave packet is well localized; see Fig. 3(a). We observe from Fig. 3(b) that for $t \sim 20$ μs, the wave packet has already spread significantly and $|\psi(\mathbf{r},t)|^2$ is delocalized along a circle in the fiber transverse plane. Figures 3(c) and 3(d) show that, when the evolution time t is about 100 μs or 200 μs, the wave packet partially relocalizes in the form of four and two subpackets, respectively. These regions are the regions of $T_{rev}/8$ and $T_{rev}/4$ fractional revivals [3,9]. According to Figs. 3(e) and 3(f), the probability density $|\psi(\mathbf{r},t)|^2$ reforms into a structure with a single dominant peak when the evolution time t is about 400 μs or 800 μs. The structure in Fig. 3(e) is the result of the half revival realized at $T_{rev}/2$. Near this time, the wave packet reforms with the original periodicity, but the phase of its orbiting motion differs from the initial wave packet [3]. The structure in Fig. 3(f) is the result of the full revival at T_{rev}. Near this time, the wave packet reforms with the original periodicity. Its peak value is reduced and its spread is increased with respect to the original wave packet due to cubic and higher

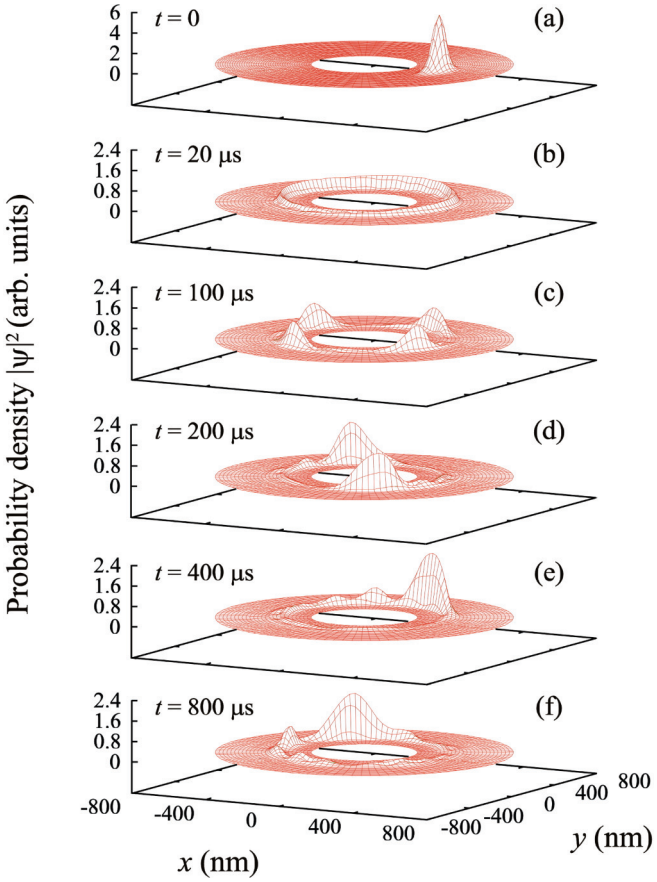

FIG. 3. (Color online) Atomic probability density $|\psi(\mathbf{r},t)|^2$ in the fiber transverse plane at different evolution times. $|\psi(\mathbf{r},t=0)|^2$ is a Gaussian wave packet of angular momentum states with $m_0 = 468$, $\Delta m = 6$, $m_{\min} = 446$, and $m_{\max} = 510$.

order terms in the dispersion relation. In the special case where $T_{\rm rev}/T_{\rm rot}$ is an integer, the full revival is in phase with the initial time development [3].

III. PROBING THE WAVE PACKET

In order to experimentally reveal the predicted wave packet dynamics, we propose to probe the orbiting atom by a weak, resonant, quasilinearly polarized guided field $\mathbf{E}_p(\mathbf{r})$ of frequency ω_p. Neglecting the effect of the fiber on the spontaneous emission rate and the detuning [14], the rate of the scattering from the atom is proportional to the overlap between the atomic wave packet and the probe field,

$$\gamma_{\rm sca}(t) \propto \int |\psi(\mathbf{r},t)|^2 |\mathbf{E}_p(\mathbf{r})|^2 d\mathbf{r}. \tag{4}$$

Assume that the main axis of the polarization of the probe guided field is aligned at the azimuthal angle $\varphi = 0$. For the following, we take advantage of the fact that the intensity of the quasilinearly polarized fundamental-mode guided probe field exhibits an azimuthal modulation according to [15]

$$|\mathbf{E}_p(\mathbf{r})|^2 \propto \left|e_\varphi^{(\omega_p)}(r)\right|^2 + \left[\left|e_r^{(\omega_p)}(r)\right|^2 - \left|e_\varphi^{(\omega_p)}(r)\right|^2 + \left|e_z^{(\omega_p)}(r)\right|^2\right]\cos^2\varphi, \tag{5}$$

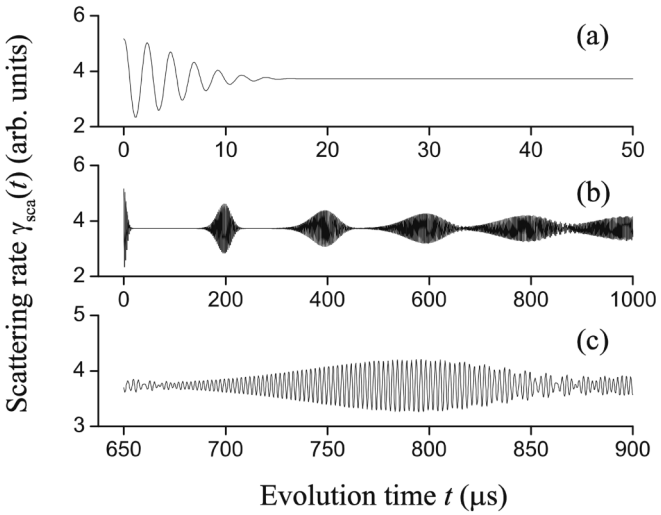

FIG. 4. Time dependence of the scattering rate $\gamma_{\rm sca}(t)$ in the ranges from 0 to 50 μs (a), from 0 to 1000 μs (b), and from 650 to 900 μs (c). The polarization of the guided probe field is aligned at the azimuthal angle $\varphi = 0$.

where $e_r^{(\omega_p)}$, $e_\varphi^{(\omega_p)}$, and $e_z^{(\omega_p)}$ are the cylindrical components of the mode profile vector function $\mathbf{e}^{(\omega_p)}$ [10,15]. Hence, we find

$$\gamma_{\rm sca}(t) \propto B + \sum_m c_{m-1}c_{m+1}V_m \cos\left(2\Delta\mathcal{E}_m t/\hbar\right), \tag{6}$$

where $\Delta\mathcal{E}_m = (\mathcal{E}_{m+1} - \mathcal{E}_{m-1})/2$ and the coefficients B and V_m are

$$B = \sum_m c_m^2 \int_a^\infty u_m^2 \left(\left|e_r^{(\omega_p)}\right|^2 + \left|e_\varphi^{(\omega_p)}\right|^2 + \left|e_z^{(\omega_p)}\right|^2\right) dr,$$
$$V_m = \int_a^\infty u_{m-1}u_{m+1}\left(\left|e_r^{(\omega_p)}\right|^2 - \left|e_\varphi^{(\omega_p)}\right|^2 + \left|e_z^{(\omega_p)}\right|^2\right) dr. \tag{7}$$

We plot in Fig. 4 the time dependence of $\gamma_{\rm sca}(t)$. Figure 4(a) shows that $\gamma_{\rm sca}(t)$ oscillates with an initial visibility of almost 40%. The oscillations result from the classical rotation of the atomic wave packet around the nanofiber. With time, the modulation amplitude reduces and $\gamma_{\rm sca}(t)$ reaches a quasistationary value for $t \sim 15$ μs. The period of oscillations of $\gamma_{\rm sca}(t)$ as obtained from the numerical evaluation is $T_{\rm osc}^{\rm (sca)} \cong 2.33$ μs, one-half of the classical atomic rotation period $T_{\rm rot} \cong 4.67$ μs. This reduction is due to the fact that the intensity of the probe field is symmetric with respect to the reflection $\{r,\varphi\} \to \{r,\varphi+\pi\}$ in the fiber transverse plane; see Eq. (5). In Fig. 4(b), clear-cut resumptions of the oscillation of the scattering rate $\gamma_{\rm sca}(t)$ appear when the evolution time is about 200 μs, 400 μs, 600 μs, and 800 μs, corresponding to $T_{\rm rev}/4$, $T_{\rm rev}/2$, $3T_{\rm rev}/4$, and $T_{\rm rev}$, respectively. As a specific characteristic of our probing scheme, the fractional revival of the wave packet at $T_{\rm rev}/8$; see Fig. 3(c), and the fractional revivals at odd multiples of $T_{\rm rev}/8$ as well as all higher order fractional revivals [3] do not give rise to a modulation of $\gamma_{\rm sca}(t)$. This can be readily understood considering the fourfold azimuthal symmetry of $|\psi(\mathbf{r},t)|^2$ for these fractional revivals. In conjunction with the $\cos^2\varphi$ dependence of the probe field intensity, one can easily show that the modulation amplitude of $\gamma_{\rm sca}(t)$ in Eq. (4) vanishes. Figure 4(c) shows a zoom of

the signal around $T_{\rm rev}$. The visibility of the scattering signal is reduced to about $1/3$ of the initial visibility, revealing the increased spread of the wave packet upon revival; see Fig. 3(f).

In order to further link the wave-packet dynamics with the predicted signal, $\gamma_{\rm sca}(t)$, we expand $\Delta\mathcal{E}_m$ in Eq. (6) into a Taylor series of the second order around the central azimuthal quantum number m_0 and find

$$\Delta\mathcal{E}_m \cong \mathcal{E}'_{m_0} + \mathcal{E}''_{m_0}(m - m_0). \tag{8}$$

The first term in Eq. (8) leads to the oscillations of the scattering rate with the period $T_{\rm osc}^{\rm (sca)} = \pi\hbar/\mathcal{E}'_{m_0} = T_{\rm rot}/2$. This period is the same for the initial and resumed oscillations of the scattering rate. Note that this also holds for the fractional revivals at $T_{\rm rev}/4$ and $3T_{\rm rev}/4$ where two diametric wave packets orbit around the nanofiber. The second term in Eq. (8) leads to the falloff and the resumptions of oscillations in the scattering rate. We define the falloff time of $\gamma_{\rm sca}(t)$ as the time at which the spread of phase differences between various oscillatory terms in Eq. (6) is about π and find $T_{\rm fall}^{\rm (sca)} = \pi\hbar/(2|\mathcal{E}''_{m_0}|\Delta m) = \sqrt{\pi}T_{\rm coll}/4$. For the resumption time of $\gamma_{\rm sca}(t)$, we obtain $T_{\rm resume}^{\rm (sca)} = \pi\hbar/|\mathcal{E}''_{m_0}| = T_{\rm rev}/4$. Based on the parameters used in our numerical calculations, we find $T_{\rm osc}^{\rm (sca)} \cong 2.33$ μs, $T_{\rm fall}^{\rm (sca)} \cong 16.5$ μs, and $T_{\rm resume}^{\rm (sca)} \cong 199$ μs, in agreement with Fig. 4.

IV. DISCUSSION

The observation of the predicted quantum dynamical effects for cold atoms orbiting in a light-induced potential surrounding an optical nanofiber is within the scope of current nanofiber-based quantum optics experiments. In particular, loading of atoms and wave-packet preparation in stable orbits around the nanofiber should be possible by starting with a stationary trap in which the repulsion of the atoms from the nanofiber surface is accomplished by means of a blue-detuned nanofiber-guided light field [7,11–13]. After laser cooling of the atoms into the vibrational ground state of the two-color optical potential, the latter can then be set into rotation using polarization modulators [16]. In this way, a repulsive centrifugal barrier is built up which consecutively replaces the repulsive blue-detuned potential, thereby transforming the two-color trap into the angular-momentum trap (see Appendix).

We like to point out the connection of our loading mechanism to experiments on optical centrifuges for molecules [17]: In both cases, the optical centrifuge and our scheme, angular momentum is added to a particle using a light field. However, the difference is that in the case of the optical centrifuge the accelerating force originates from the strong-field alignment of the anisotropic particles whereas in the situation described here, (isotropic) atoms are accelerated by specifically employing the optical dipole force of a light field with an azimuthally varying intensity.

The proposed system can be seen as a two-dimensional "artificial atom" where the orbiting atom and the nanofiber take the role of the valence electron and the ion core, respectively, while the Coulomb attraction is replaced by a tunable light-induced potential. In view of the tunability of the dispersion relation, this would then implement a versatile experimental platform for the investigation of quantum wave-packet dynamics.

ACKNOWLEDGMENTS

We thank I. Brezinova, J. Burgdörfer, J. I. Cirac, J. Dalibard, J.-F. Schaff, and S. Yoshida for helpful comments and discussions. Financial support from the European Science Foundation (EURYI Award), the Wolfgang Pauli Institute, and the Austrian Science Fund (FWF; Lise Meitner Project No. M 1501-N27 and SFB NextLite Project No. F 4908-N23) is gratefully acknowledged.

APPENDIX: TRAP LOADING AND WAVE-PACKET PREPARATION

A possible experimental sequence to load the trap and to prepare the initial wave packet in our system is shown in Fig. 5. The sequence consists of a smooth transformation of the two-color trap [12], followed by an abrupt switching of the optical potentials. The dotted black line in Fig. 5(a)

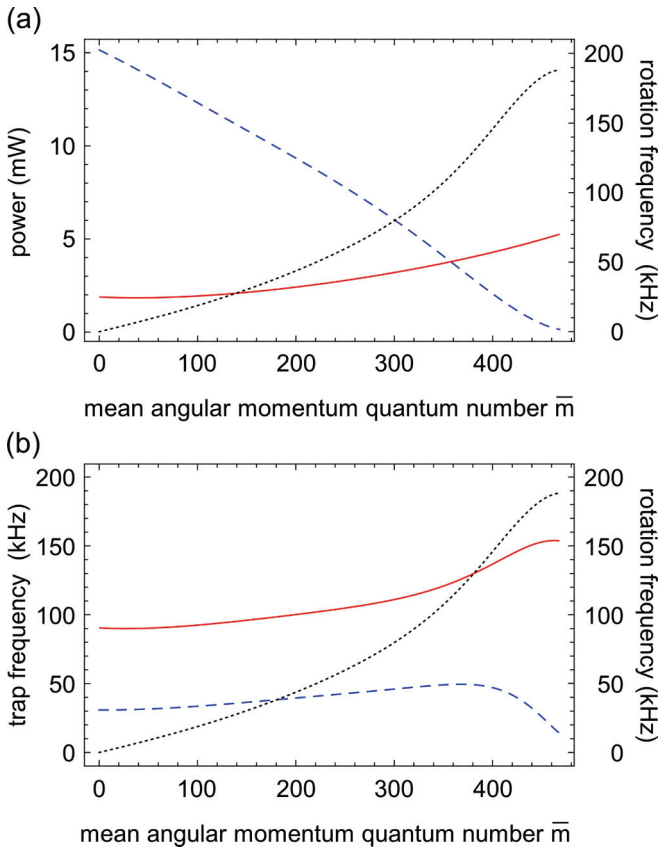

FIG. 5. (Color online) Smooth transformation of the trapping potential. (a) (Solid red and dashed blue lines) Optical powers of the red- and blue-detuned trapping fields, respectively; (dotted black line) rotational frequency of the polarization plane of the blue-detuned trapping field. (b) (Solid red and dashed blue lines) Radial and azimuthal trapping frequencies, respectively; (dotted black line) rotational frequency of the polarization plane of the blue-detuned trapping field. All quantities are given as a function of the mean angular momentum quantum number $\bar{m}$. The parameters of the nanofiber are identical to what is assumed in the main text.

shows the rotation frequency f of the polarization plane of the blue-detuned trapping field while its power is indicated by the dashed blue line. Both quantities are given as a function of the mean angular momentum quantum number $\bar{m}$. The rotation frequency is monotonously increased, reaching $f \approx 190$ kHz at the end of the smooth transformation. The corresponding mean angular momentum matches $m_0 = 468$, as assumed in the main manuscript. We note that f is not linearly proportional to $\bar{m}$ because the radial distance of the trapping minima slightly varies during the sequence.

The power of the blue-detuned laser is reduced from about 15 mW to about 0.15 mW. This final power of the blue-detuned laser provides sufficient azimuthal confinement such that the azimuthal width of the initial wave function matches the width of the wave packet shown in Fig. 3(a) of the main manuscript, corresponding to a final azimuthal trap frequency ≈ 15 kHz [see the dashed blue line in Fig. 5(b)]. In order to release the prepared wave packet into the angular momentum trap, the blue-detuned laser and, thus, the azimuthal confinement are abruptly switched off. The wave packet will then propagate freely and undergo collapse and revival dynamics.

For the above sequence, the red-detuned trapping field is chosen in a standing wave configuration in order to ensure axial confinement of the atoms. The power of this field is continuously adjusted [Fig. 5(a), solid red line]. This ensures that the trapping potential is sufficiently deep throughout the entire sequence and that the radial position of the two-color trap matches the radial position of the angular-momentum trap at the end of the smooth variation.

In order to start the loading sequence with a well-defined center-of-mass wave function, the atoms have to be prepared in their motional ground state which is possible using standard side-band cooling techniques [18,19]. The trap transformation is then ideally carried out in such a way that no vibrational excitation is present just before abruptly switching the trapping fields. This either calls for an adiabatic transformation of the potentials [20] or for a nonadiabatic optimal control sequence [21]. In both cases, the implementation requires the specification of a suitable temporal variation of the experimental parameters as a function of time. In particular, the rotation frequency $f(t)$ has to be defined. Evaluating the vibrational excitation probability for a given $f(t)$ implies solving the time-dependent three-dimensional Schrödinger equation for the time-varying trapping potential over the entire sequence and is beyond the scope of this work. A first analysis of the classical stability of the trap during the variation of the rotation frequency indicates that a region of instability can occur if the rotation frequency lies between the radial and the azimuthal trapping frequencies [22]. In order to minimize the resulting vibrational excitation, a compromise between a slow variation of the trap parameters and a fast crossing of the instability region has to be found. The latter will profit from approaching the radial and the azimuthal trapping frequencies. In particular, when the trapping frequencies are equal, even an adiabatic variation can be implemented. Under these circumstances, the collapse and revival dynamics should prevail and should be observable with the method that is proposed in the main text.

[1] E. Schrödinger, Naturwissenschaften **14**, 664 (1926).

[2] J. Parker and C. R. Stroud, Jr., Phys. Rev. Lett. **56**, 716 (1986); Phys. Scr. T **12**, 70 (1986).

[3] R. W. Robinett, Phys. Rep. **392**, 1 (2004).

[4] S. Will, T. Best, U. Schneider, L. Hackermüller, D.-S. Lühmann, and I. Bloch, Nature (London) **465**, 197 (2010).

[5] B. Wyker, S. Ye, F. B. Dunning, S. Yoshida, C. O. Reinhold, and J. Burgdörfer, Phys. Rev. Lett. **108**, 043001 (2012).

[6] O. D. Skoromnik, I. D. Feranchuk, and C. H. Keitel, Phys. Rev. A **87**, 052107 (2013).

[7] J. P. Dowling and J. Gea-Banacloche, Adv. At. Mol. Opt. Phys. **37**, 1 (1996).

[8] V. I. Balykin, K. Hakuta, F. L. Kien, J. Q. Liang, and M. Morinaga, Phys. Rev. A **70**, 011401(R) (2004).

[9] I. Sh. Averbukh and N. F. Perelman, Phys. Lett. **139**, 449 (1989).

[10] A. W. Snyder and J. D. Love, *Optical Waveguide Theory* (Chapman and Hall, New York, 1983).

[11] Fam Le Kien, V. I. Balykin, and K. Hakuta, Phys. Rev. A **70**, 063403 (2004).

[12] E. Vetsch, D. Reitz, G. Sagué, R. Schmidt, S. T. Dawkins, and A. Rauschenbeutel, Phys. Rev. Lett. **104**, 203603 (2010).

[13] A. Goban, K. S. Choi, D. J. Alton, D. Ding, C. Lacroûte, M. Pototschnig, T. Thiele, N. P. Stern, and H. J. Kimble, Phys. Rev. Lett. **109**, 033603 (2012).

[14] Fam Le Kien, S. Dutta Gupta, V. I. Balykin, and K. Hakuta, Phys. Rev. A **72**, 032509 (2005).

[15] Fam Le Kien, J. Q. Liang, K. Hakuta, and V. I. Balykin, Opt. Commun. **242**, 445 (2004).

[16] A. La Porta and M. D. Wang, Phys. Rev. Lett. **92**, 190801 (2004).

[17] J. Karczmarek, J. Wright, P. Corkum, and M. Ivanov, Phys. Rev. Lett. **82**, 3420 (1999).

[18] A. M. Kaufman, B. J. Lester, and C. A. Regal, Phys. Rev. X **2**, 041014 (2012).

[19] J. D. Thompson, T. G. Tiecke, A. S. Zibrov, V. Vuletic, and M. D. Lukin, Phys. Rev. Lett. **110**, 133001 (2013).

[20] D. Comparat, Phys. Rev. A **80**, 012106 (2009).

[21] H. Mabuchi and N. Khaneja, Int. J. Robust Nonlin. **15**, 647 (2005).

[22] S. Yoshida, I. Brezinova, and J. Burgdörfer (private communication).